Back to Session Subjects

Modeling Dynamic Equations of Motion of a Composite Hingeless Helicopter Rotor Blade

B. Bailey*, F. Afagh† and F. Nitzsche‡

Abstract

The first-order nonlinear equations of motion for a composite, thin-walled, multi-celled hingeless rotor blade with integral actuators are developed. This is done by using the variational asymptotic method to find cross-sectional expressions for the beam stiffness, strain field and shell energy. Integrating the shell energy over the blade length results in the linear strain energy density. This is used in Hamilton's Equation to find the equations of motion and related boundary conditions. These equations are solved using Galerkin's Method for non-linear steady-state and linearized perturbation.

1 Introduction

Hinges are incorporated into helicopter blade design to reduce the high bending moments at the root, but result in a lag in the response time. With the advent of composite materials, there is an initiative to develop hingeless blades. Recent advances in active materials technology allow for a potential means of vibration and pitch angle control.

Helicopter rotor blade analysis is a complex subject that encompasses aerodynamics, structures and composite materials. The ability to control the coupling between deformation modes through the orientation of the fibers allows for the tailoring of helicopter blade dynamics. Piezoelectric fibers, which strain under the application of an electric field, can be embedded into the composite and allow for anisotropic actuation.

This paper provides an aeroelastic analysis of a hingeless helicopter rotor blade with active fibers in hover. The analysis is limited to the case of constant cross-sectional properties and no cordwise offset between the elastic, mass, tension and aerodynamic axes.

2 Cross-Sectional Analysis

The analysis of the helicopter rotor blade can be broken down into a linear two-dimensional analysis of the cross-section, and a non-linear analysis along the blade span. The cross-section is modeled by the variational asymptotic method [1]. This method is an iterative process of approximating the displacements and finding the associated shell energy. The displacement terms with a contribution of less than two orders of magnitude, compared to the largest in the shell energy, are ignored. The process is terminated when the new terms do not produce terms of the same order as the rest in the shell energy. This process will asymptotically approach the shell energy contained in a thin-walled beam. Thus, closed-form expressions for the displacement and stress fields, and beam stiffness coefficients result from this analysis.

This method was further developed to include anisotropic closed-cross-section beams [2], expanded to include two-cell composite beams [3], and further refined to include anisotropic actuation [4] . A schematic of this method is given in Figure 1, and corrections to stiffness terms for a two-celled beam with integral actuation are given in Appendix A.

The constitutive relations obtained from this method can be written in matrix form as:

$$\begin{pmatrix} F_1 \\ M_1 \\ M_2 \\ M_3 \end{pmatrix} = [K]_{4\times 4} \begin{pmatrix} U_1' \\ \varphi' \\ -U_3'' \\ U_2'' \end{pmatrix} - \begin{pmatrix} F_1^{(a)} \\ M_1^{(a)} \\ M_2^{(a)} \\ M_3^{(a)} \end{pmatrix}$$

where F_1, M_1, M_2 and M_3 are the traction, torsional moment, flap bending moment and lead-lag bending moment, respectively. U_1, U_2 and U_3 represent the average cross-sectional translations in the axial, lead-lag and flap directions, respectively, and φ is the torsional rotation. The cross-sectional stiffness terms K_{ij} are dependent upon the blade geometry and material properties, and the matrix is symmetric. The corrected

*Graduate Research Assistant, †Professor and ‡Associate Professor at Department of Mechanical and Aerospace Engineering, Carleton University, Ottawa, Canada.

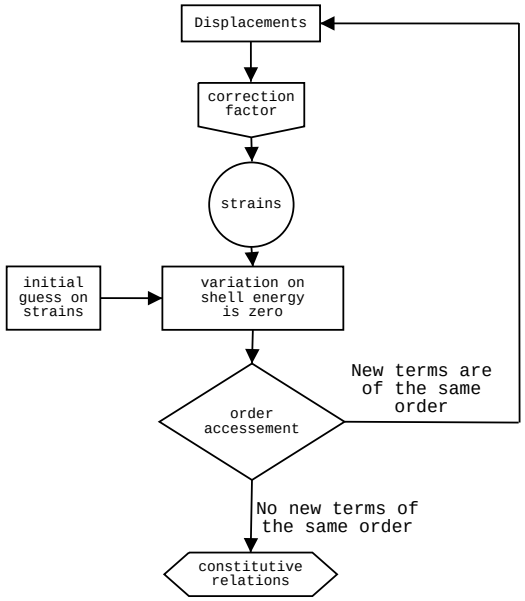

Figure 1: Variational asymptotic method.

actuation terms are given in Appendix A.

3 Nonlinear Beam Analysis

Integrating the shell energy over the blade length gives the strain energy, which is used in Hamilton's equation :

$$\int_{t_1}^{t_2} \left[\delta\left(U-T\right)-\delta W\right] dt = 0$$

where U is the strain energy, T is the kinetic energy and δW is the virtual work due to the external forces. The only external forces considered in this approach are due to aerodynamic loading. The corresponding kinetic energy and virtual work terms are obtained in [5].

The shell energy functional Φ per unit middle surface area, obtained from the variational asymptotic method, integrated over the cross-section and blade length L gives the strain energy. Hence,

$$U = \int_0^L \int_{all} \Phi \; ds \; dx$$

where the cross-sectional coordinate is s and the axial coordinate is x.

Taking the variation of the strain energy, and replacing the shell energy functional with the constitutive relations, the following is obtained:

$$\delta U = \int_0^L \left[F_1 \delta U_1' + M_1 \delta\varphi' - M_2 \delta U_3'' + M_3 \delta U_2''\right] dx$$

The displacements and strains are transformed from the local, cross-sectional b to a global a coordinate system, as shown in Figure 2. This is done by using the coordinate transformations given by [6].

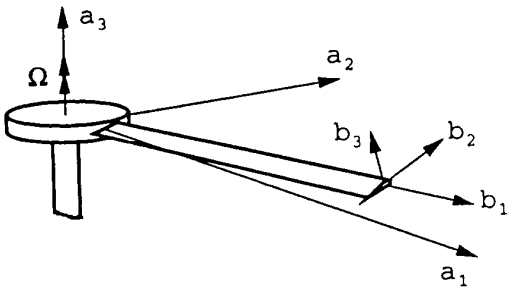

Figure 2: Coordinate systems, from [7] .

Integration by parts is then applied to give all of the variations in terms of global displacements only, eliminating variations of the derivatives. This results in four variational equations in the global coordinate system, with respect to the axial u, torsional φ, lead-lag v and flap w displacements, and their associated boundary conditions. As the variations are arbitrary, but admissible, and the integrals equal to zero, the integrands must vanish. The four integrands equaling to zero are the four equations of motion of the blade.

The equation of motion associated with the variation of the axial displacement can be used to eliminate the axial displacement as an independent variable. This results in three equations of motion and boundary conditions, which can be nondimensionalized. The terms are ranked according to their degree of nonlinearity, and only up to the first order nonlinear terms are kept.

The non-dimensionalized equations of motion are as follows:

$\delta\bar{v}$ equation

$$\begin{aligned}
&-\Pi_1 - \Pi_2\bar{\varphi} + \Gamma_1\bar{v}'''' + \Gamma_3\bar{v}''''\bar{\varphi} + \Gamma_3\left(\bar{v}\bar{\varphi}\right)'''' \\
&-\Gamma_3\bar{w}'''' + \Gamma_2\bar{w}''''\bar{\varphi} + \Gamma_1\left(\bar{w}\bar{\varphi}\right)'''' + \Upsilon_1\bar{\varphi}''' \\
&-2\left(\dot{\bar{v}}'\bar{v} + \left(\dot{\bar{v}}\bar{v}\right)' + \beta_{pc}\dot{\bar{w}} + \tfrac{\Lambda_{12}}{\Lambda_{11}}\dot{\bar{\varphi}} - \Pi_2\dot{\bar{w}}' + \left(\dot{\bar{w}}\bar{w}\right)'\right) \\
&+\Upsilon_2\bar{\varphi}\bar{\varphi}''' - 2\bar{v} - 4\Pi_1\dot{\bar{v}}' + \ddot{\bar{v}} + \Pi_1\bar{F}_1^{(a)\prime\prime} \\
&-\bar{M}_3^{(a)\prime\prime}\cos\theta - \bar{M}_2^{(a)\prime\prime}\sin\theta = \bar{L}_v
\end{aligned}$$

$\delta\bar{w}$ equation

$$\Pi_2 - \Pi_1\bar{\varphi} - \Gamma_3\bar{v}'''' + \Gamma_1\bar{v}''''\bar{\varphi} + \Gamma_2\left(\bar{v}\bar{\varphi}\right)'''' - \Gamma_2\bar{w}'''' - \Gamma_3\bar{w}''''\bar{\varphi} - \Gamma_3\left(\bar{w}\bar{\varphi}\right)'''' - \Upsilon_2\bar{\varphi}''' + \Upsilon_1\bar{\varphi}\bar{\varphi}''' + 2\Pi_2\dot{\bar{v}}' - \bar{w} - 2\dot{\bar{v}}'\bar{w} + \beta_{pc}\left(\bar{x} + 2\dot{\bar{v}}\right) + \ddot{\bar{w}} - \Pi_2\bar{F}_1^{(a)\prime\prime} - \bar{M}_3^{(a)\prime\prime}\sin\theta - \bar{M}_2^{(a)\prime\prime}\cos\theta = \bar{L}_w$$

$\delta\bar{\varphi}$ equation

$$\left(\frac{\Lambda_{12}^2}{\Lambda_{11}} - \Lambda_{22}\right)\bar{\varphi}'' + \frac{\Lambda_{12}}{\Lambda_{11}}\left(\bar{x} + 2\dot{\bar{v}}\right) - \Upsilon_1\bar{v}''' + \Upsilon_2\bar{w}''' - \Pi_2\bar{v} - \Pi_1\bar{w} + \Upsilon_2\left(\bar{v}\bar{\varphi}''' - \left(\bar{v}\bar{\varphi}\right)'''\right) + \Upsilon_1\left(\bar{w}\bar{\varphi}''' - \left(\bar{w}\bar{\varphi}\right)'''\right) + \Gamma_3\bar{v}\bar{v}'''' + \Gamma_1\bar{w}\bar{v}'''' - \Gamma_3\bar{w}\bar{w}'''' + \Gamma_2\bar{v}\bar{w}'''' + \mu^2\ddot{\bar{\varphi}} + \tfrac{1}{2}\left(\mu_2^2 - \mu_1^2\right)\sin 2\theta + \left(\mu_2^2 - \mu_1^2\right)\bar{\varphi}\cos 2\theta + \bar{M}_1^{(a)\prime} - \frac{\Lambda_{12}}{\Lambda_{11}}\bar{F}_1^{(a)\prime\prime} = \bar{M}_\varphi$$

where $\bar{v}$ and $\bar{w}$ are the lead-lag and flap displacements nondimensionalized by the blade length, respectively. $\bar{\varphi}$, θ and β_{pc} are the torsion twist, pitch angle and precone about the axial axis, respectively. The nondimensionalized variables are given in Appendix B.

3.1 Solution to the Equations

The equations of motion are solved by applying Galerkin's Method. In this method, the displacements are represented as an infinite series of generalized coordinates and mode shape functions:

$$\bar{v} = \sum_{j=1}^{N} V_j\left(\psi\right)\Psi\left(\bar{x}\right)$$

$$\bar{w} = \sum_{j=1}^{N} W_j\left(\psi\right)\Psi\left(\bar{x}\right)$$

$$\bar{\varphi} = \sum_{j=1}^{N} \phi_j\left(\psi\right)\Theta\left(\bar{x}\right)$$

$\bar{x}$ is the axial coordinate nondimensionalized with respect to the blade length. ψ is the azimuth angle, a nondimensionalized time which is equal to the angular velocity Ω of the blade multiplied by time. V_j, W_j and ϕ_j are the generalized coordinates, and Ψ and Θ are the mode shape in bending and torsion, respectively.

The mode shapes used are the standard, uncoupled mode shapes of a non-rotating cantilevered beam. Integration by parts is applied to the Galerkin equations, which satisfies the natural and imposed boundary conditions.

3.2 Steady State and Perturbation

The generalized modal coordinates can be broken down into steady-state and perturbation values :

$$V_j = V_{0j} + \Delta V_j$$
$$W_j = W_{0j} + \Delta W_j$$
$$\phi_j = \phi_{0j} + \Delta\phi_j$$
$$E_e = E_{e0} + \Delta E_e$$

This allows for the separation of the equations of motion into steady state and perturbation equations. The steady state equations given in Appendix D, can be solved by many different nonlinear techniques (such as the Newton-Raphson Method). The perturbation equations are then linearized about the steady state values, which results in a homogeneous ordinary differential equation in the familiar form :

$$[M]\left\{\ddot{X}\right\} + [C]\left\{\dot{X}\right\} + [K]\{X\} + \{F\}\Delta E_e = 0$$

where $[M]$, $[C]$ and $[K]$ are the mass, damping and stiffness matrices, respectively. The $\{F\}$ vector is an actuation input, and $\{X\}$ is a column vector composed of the flap, lag and torsion perturbation generalized deflections.

$$\{X\} = \begin{Bmatrix} \Delta V_j \\ \Delta W_j \\ \Delta\phi_j \end{Bmatrix}$$

The damping matrix $[C]$ and the stiffness matrix $[K]$ are divided into aerodynamic, $[C_a]$ and $[K_a]$, and structural, $[C_s]$ and $[K_s]$, respectively. The values for all of these matrices can be found in Appendix E.

4 Aeroelastic Analysis

The aeroelastic stability analysis is presented for two different spar designs: a baseline composite box-beam spar without active fibers and a composite box-beam spar containing piezoelectric fibers in the circumferential walls. The steady-state response is then found for the baseline spar and for the spar containing the piezoelectric fibers with no applied electric field and with the maximum electric field applied. The perturbation response is obtained for the three preceding cases, and a simple optimization is used for the dynamic control.

These results were obtained from computer codes that run in the MATLAB^{TM} Version 5.3 environment using 6 mode shapes.

4.1 Design of Spar

A baseline test spar was designed for a Westland WG13 helicopter, whose basic properties are presented in Table 1. The additional mass of steel rods placed at the blade's leading and trailing edges are used to tune the four lowest frequencies to approximately those of a typical helicopter rotor blade (at about 1/rev, 2/rev, 2.5/rev and 3.5/rev). These weights are sectioned off into small lengths to change the mass and inertial

properties of the blade without increasing the stiffness.

Number of blades, b	4
Blade chord, c	0.394 m
Main rotor radius, L	7.52 m
Coefficient of drag, C_D	0.011
Tip velocity, ΩL	213.4 m/s

Table 1: Properties of Westland WG13 helicopter [8].

The cross-sectional dimensions of the spar are given in Figure 3. This spar can be contained inside a NACA 0020 airfoil, which is thicker than most conventional helicopter rotor blades. This is done to avoid flutter when the extra mass due to the piezoelectric fibers is included. Therefore, as the flapping mode was dominant in this flutter case, the height of the spar was increased to augment the flapping stiffness K_{33}.

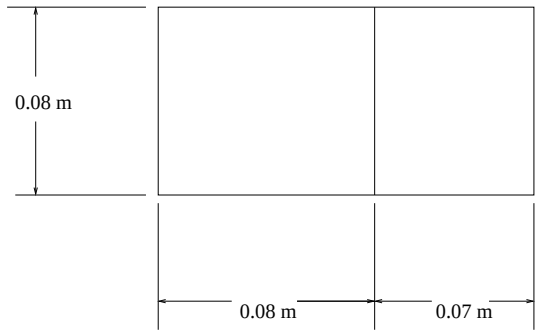

Figure 3: Dimensions of Baseline boxbeam spar.

The baseline spar is composed of layers of AS4/3506-1 Carbon/Epoxy, the material properties of which can be found in Table 3. The number of plies and their corresponding angles for the horizontal and vertical walls are given in Table 2. The resulting stiffness terms for the boxbeam are presented in Table 4.

Member	*Orientation*
horizontal	$[-45,+45,0,-45,+45,0,-45,+45]_2$
vertical	$[-45,+45,0,-45,+45,0,-45,+45]$

Table 2: Orientation of AS4/3506-1 Graphite/Epoxy plies for Baseline spar.

As mentioned earlier, the frequencies of the spar were tuned to approximate those of a real helicopter rotor blade using weights placed close to the leading and trailing edges. As the present analysis assumes no chordwise offset of the elastic and mass axes, the round tuning rods are made from the same material, have the same radius (2mm) and are placed equidistant from the centroid (0.17m).

The Active Fiber Composite (AFC) spar is identical to the baseline spar, except that it contains a single layer of PZT-5H piezoelectric fiber in the circumferential members. The material properties of the active fiber are given in Table 3. In order to maximize the actuation force in twist ($M_1^{(a)}$), the piezoelectric fibers are aligned at $+45°$.

	AS4/3506-1	*PZT-5H*
E_{LL} (GPa)	142	30.2
$E_{NN} = E_{TT}$ (GPa)	9.8	14.9
$G_{LT} = G_{LN}$ (GPa)	6.0	5.13
G_{TN} (GPa)	4.8	3.6
$\nu_{LT} = \nu_{LN}$	0.30	0.45
ν_{TN}	0.42	0.40
Thickness (mm)	0.127	0.17
Density (kg/m^3)	1790	4060
d_{LLL} (pm/V)	0	309
d_{LTT} (pm/V)	0	-129
d_{LNN} (pm/V)	0	-0.129

Table 3: Properties of AS4/3506-1 graphite/epoxy and PZT-5H piezoelectric fiber where L is along the fiber direction, N is normal to the laminate and T is orthogonal to L and N.

The piezoelectric fiber layer creates a coupling stiffness B in the circumferential members, which results in extension-torsion coupling K_{12} and torsion-bending coupling K_{24}. The resulting stiffnesses and inertial terms are presented with the baseline case in Table 4.

	Baseline Spar	*AFC Spar*
K_{11} (N)	4.40×10^7	4.53×10^7
K_{12} (Nm)	0	5.26×10^3
K_{14} (Nm)	-2.10×10^4	-2.10×10^4
K_{22} (Nm^2)	5.48×10^4	5.69×10^4
K_{24} (Nm^2)	0	4.90
K_{33} (Nm^2)	5.70×10^4	5.86×10^4
K_{44} (Nm^2)	1.06×10^5	1.10×10^5
m (kg/m)	1.72	2.04
k_{m1} (m)	0.935	0.935
k_{m2} (m)	0.0693	0.0703

Table 4: Non-zero stiffnesses, mass per unit length and radii of gyration for the Baseline and AFC spar.

As the lengths and ply angles of the top and bottom piezoelectric fiber layers are the same, the forces will cancel out each other, and the activa-

tion moment $M_3^{(a)}$ will be zero. The same reasoning applies to the left and right walls and to the $M_2^{(a)}$ activation moment. This leaves only two components of the activation vector, $F_1^{(a)}$ and $M_1^{(a)}$, which are given in Table 5 for an induced electric field of -1800 V/ 1.114 mm.

$F_1^{(a)}$ (N)	- 1.00×10^0
$M_1^{(a)}$ (Nm)	-1.28×10^{-1}
$M_2^{(a)}$ (Nm)	0
$M_3^{(a)}$ (Nm)	0

Table 5: Forcing vector terms for active spar with an induced electric field of -1800 V/1.114mm.

4.2 Steady-State Response

The steady-state deflections, also known as trim deflections, of the rotor blade must be determined first. They also define the operating conditions of the rotor, as the thrust produced is dependent upon the total blade angle, $\theta + \varphi_0$. The results are obtained as dimensionless deflections along the blade length for one operating condition, when the pitch angle θ is equal to 0.1 radians and no precone exists.

Although the piezoelectric fiber will be distributed throughout the length of the blade, only a certain segment will be actuated. This can be accomplished by locating the interdigitated electrodes only in the chosen segment. In order to excite the desired mode shapes most effectively, the site of actuation segment becomes an important design issue. Therefore, the segment should be chosen in regions of high average strain and away from regions of zero strain [9]. Since the torsional mode is the one that is required to be controlled, only the torsion contribution to the strain is considered. Figure 4 gives the relative torsional strain distribution along the beam. To control pitch angle, the actuation segment was chosen in a region of high torsional strain and presented in Table 6.

Start point	0.025
End point	0.1

Table 6: Start and end points of the actuated segment nondimensionalized with respect to blade length for steady-state actuation.

The nondimensional deflections along the blade length are presented in Figure 5 for a pitch angle of 0.1 radians and no precone. Only the baseline case and the case of the non-activated

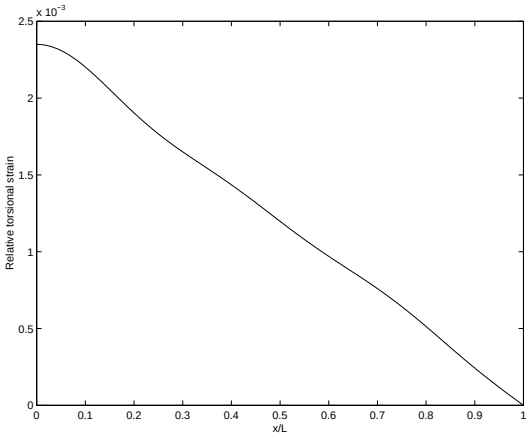

Figure 4: Relative steady-state torsional strain distribution when $\theta = 0.1$ radians and $\beta_{pc} = 0$.

AFC blade are presented in this figure. This is because the magnitude of the forcing vector for the AFC blade (Table 5) is much smaller than the stiffness values (Table 4). Hence, there is no discernible change in the trim deflections of the non-activated AFC blade from the fully-activated case where the maximum electric field (-1800 V / 1.114 mm) is applied to the chosen segment.

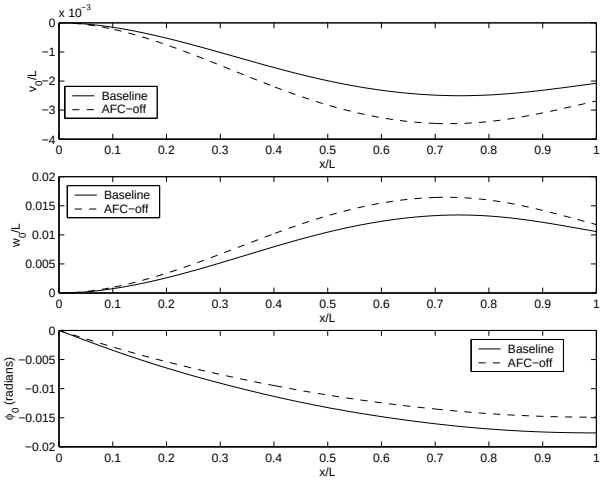

Figure 5: Steady-state deflections for the baseline spar and the spar containing the AFC fibers, not activated, when $\theta = 0.1$ radians and $\beta_{pc} = 0$.

The above results differ from other published data, such as the results reported on a 1/6th Mach-scaled Chinook CH47-D active blade by [10]. The CH47-D blade contains a D-shaped spar, where the arc is composed of 3 plies of E-glass, 2 plies of Graphite S-glass and 3 plies of AFC actuators, and the web is composed of 3 layers of E-glass. The experimental results for the latter blade are over 2°/m peak-to-peak twist

actuation. These results, however, were obtained for a non-rotating blade, and therefore did not have to deal with inertial forces or aerodynamic loading on the blade. Moreover, they were generated with 3 plies of active fibers, the extra mass of which would cause flutter. The number of active layers would have to be increased to achieve the same results on a full-scale blade.

4.3 Perturbation Response

The six lowest frequency eigenvalues of the different test cases examined in the preceding section are given in Table 7. The real part of the eigenvalues is a measure of the damping ratio, where a negative value represents a stable condition. The magnitude of the imaginary part of the eigenvalue is the aeroelastic modal frequency per revolution of the mode. The frequencies of the baseline case are in good agreement with those of typical helicopter rotor blades, except for the frequency of the second mode being half as large. This is not considered a problem, as the typical rotor blade frequencies are only a guideline and change for different blade designs.

	Baseline Spar	*AFC spar - off/static*
1^{st}	- 0.043 ± 0.965 i	- 0.156 ± 0.868 i
2^{nd}	- 0.228 ± 0.991 i	- 0.108 ± 0.894 i
3^{rd}	- 0.022 ± 2.609 i	- 0.019 ± 2.863 i
4^{th}	- 0.288 ± 3.171 i	- 0.303 ± 3.030 i
5^{th}	- 0.003 ± 3.796 i	- 0.003 ± 3.609 i
6^{th}	- 0.231 ± 7.192 i	- 0.235 ± 6.739 i

Table 7: Eigenvalues for the different designs of the rotor blade at a pitch angle of $\theta = 0.1$ radians.

It should be noted that not only was the static activation unable to modify the steady-state deflections, but it was also unable to affect the dynamic response.

For vibration control, the frequencies to be eliminated are those that get transferred to the airframe. The hub filtering and the lower frequency restriction allows for the limiting of our control strategy to the b per revolution frequency. From Table 7, the 4^{th} and 5^{th} dynamic modes for the non activated AFC spar are those closest to this criteria. Figure 6 gives the relative torsional strain distribution due to the perturbation response. As the frequency of the 5^{th} mode is closer to the b/rev frequency and there is little damping for this mode, it would cause the largest excitation of the airframe. This mode is therefore the most logically eliminated using the piezoelectric fibers. From Figure 6, the maximum strain for the 5^{th} mode is located at about 0.7 of the blade length. The actuation segment location for dynamic control is presented in Table 8.

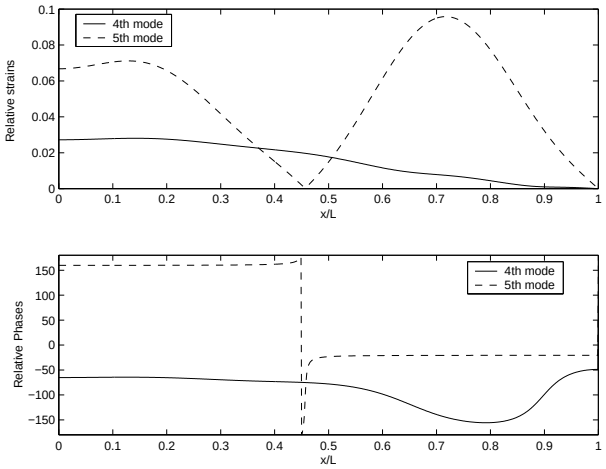

Figure 6: Torsional perturbation strain distribution for the AFC blade when $\theta = 0.1$ radians and $\beta_{pc} = 0$.

Start point	0.65
End point	0.75

Table 8: Start and end points of the actuated segment nondimensionalized with respect to blade length for dynamic actuation.

A Linear Quadratic Regulator [11] was developed to control the 5^{th} dynamic mode. This was accomplished by setting the diagonal terms associated with the 5^{th} dynamic mode in the *state weighting* matrix to one, while all other terms are zero. The resulting gain vector contains only two entries, corresponding to the two eigenvalues of the 5^{th} mode, 0.3740×10^{-7} and 0.0216×10^{-7}. The six lowest frequency eigenvalues for the dynamically controlled case are given in Table 9.

	AFC spar - dynamic
1^{st}	- 0.156 ± 0.868 i
2^{nd}	- 0.108 ± 0.894 i
3^{rd}	- 0.019 ± 2.863 i
4^{th}	- 0.303 ± 3.030 i
5^{th}	- 0.003 ± 3.609 i
6^{th}	- 0.235 ± 6.739 i

Table 9: Eigenvalues for dynamically controlled rotor blade at a pitch angle of $\theta = 0.1$ radians and no precone.

As the eigenvalues for the AFC blade without any activation (Table 7) were not changed by the addition of the control system, it is concluded

that the piezoelectric fibers do not have enough actuation authority for vibration control.

5 Conclusions

The following conclusions can be drawn from this analysis:

- The first-order nonlinear closed-form equations of motion for a hingeless helicopter rotor blade were developed. As they are based on the variational asymptotic method, they include warping and coupling between the strains. This method uses continuous functions, which represent torsional interactions better than lumped parameter methods such as the finite element method.
- The piezoelectric fibers do not have enough actuation authority for pitch angle or vibration control. When the piezoelectric fibers had a maximum steady-state voltage applied, the pitch angle of the blade was not affected. An optimal controller was designed to affect a vibration mode, but the level of actuation proved to be much lower than required. This is due to the fact that the stiffness associated with a full-scale helicopter blade is much larger than the level of actuation provided by the active fibers. The greater density of the fibers increases the total weight of the blade, which can lead to instability. Therefore, the addition of piezoelectric fibers does not alleviate the problem but increases it.

References

[1] V.L. Berdichevsky. Variational-asymptotic method of constructing a theory of shells. *PMM*, 43(4):711–736, 1979.

[2] V.L. Berdichevsky, E. Armanios, and A. Badir. Theory of anisotropic thin-walled closed-cross-section beams. *Composites Engineering*, 2(5-7):441–432, 1992.

[3] A.M. Badir. Analysis of two-cell composite beams. In *Proceedings of the 36th Structures, Structural Dynamics, and Materials Conference*, pages 419–424, 1995.

[4] C.E.S. Cesnik and S.J. Shin. Structural analysis for designing rotor blades with integral actuators. Technical Report AIAA-98-2107, AIAA, April 1998.

[5] D.H. Hodges and R.A. Ormistion. Stability of elastic bending and torsion of uniform cantilever rotor blades in hover with variable structural coupling. Contract Report TN D-8192, NASA, April 1976.

[6] D.H. Hodges and E.H. Dowell. Nonlinear equations of motion for the elastic bending and torsion of twisted nonuniform rotor blades. Contract Report TN D-7818, NASA, 1974.

[7] X. Shang and D.H. Hodges. Aeroelastic stability of composite rotor blades in hover. In *Proceedings of the 36th Structures, Structural Dynamics, and Materials Conference*, pages 2602–2610, 1995.

[8] Newman. *The Foundations of Helicopter Flight*, volume 1.0. Halsted Press, London, England, 1994.

[9] E.F. Crawley and J. de Luis. Use of piezoelectric actuators as elements of intelligent structures. *AIAA Journal*, 25(10):1373–1385, October 1987.

[10] C.E.S. Cesnik and M. Ortega-Morales. Active composite beam cross-sectional modeling - stiffness and active force constants. Technical Report AIAA-99-1548, AIAA, April 1999.

[11] B. Friedland. *Control System Design: An Introduction to State-Space Methods*, volume 1. McGraw-Hill, Boston, Massachusetts, 1986.

A Stiffness and actuation

The stiffness coefficients K_{ij} in terms of cross-sectional geometry and material properties are as follows:

$$
\begin{aligned}
K_{11} &= \int_{all} \left(A - \frac{B^2}{C}\right) ds - 4a_3 \oint_I \frac{B}{C} ds \\
&\quad -4a_4 \oint_{II} \frac{B}{C} ds \\
K_{12} &= -4a_1 \oint_I \frac{B}{C} ds - 4a_2 \oint_{II} \frac{B}{C} ds \\
K_{13} &= \int_{all} \left(A - \frac{B^2}{C}\right) z ds + 4a_7 \oint_I \frac{B}{C} ds \\
&\quad +4a_8 \oint_{II} \frac{B}{C} ds
\end{aligned}
$$

$$
\begin{aligned}
K_{14} &= -\int_{all}\left(A-\frac{B^2}{C}\right)yds-4a_5\oint_I\frac{B}{C}ds \\
&\quad -4a_6\oint_{II}\frac{B}{C}ds \\
K_{22} &= -4a_1A_{eI}-4a_2A_{eII} \\
K_{23} &= 4a_7A_{eI}+4a_8A_{eII} \\
K_{24} &= -4a_5A_{eI}-4a_6A_{eII} \\
K_{33} &= \int_{all}\left(A-\frac{B^2}{C}\right)z^2ds+4a_7\oint_I\frac{B}{C}zds \\
&\quad +4a_8\oint_{II}\frac{B}{C}zds \\
K_{34} &= -\int_{all}\left(A-\frac{B^2}{C}\right)zyds-4a_5\oint_I\frac{B}{C}zds \\
&\quad -4a_6\oint_{II}\frac{B}{C}zds \\
K_{44} &= \int_{all}\left(A-\frac{B^2}{C}\right)y^2ds+4a_5\oint_I\frac{B}{C}yds \\
&\quad +4a_6\oint_{II}\frac{B}{C}yds
\end{aligned}
$$

and the corresponding contributions from the piezoelectric fibers are given by:

$$
\begin{aligned}
F_1^{(a)} &= \int_{all}\left(A^{(a)}-\frac{B}{C}C^{(a)}\right)ds \\
&\quad +2g_1^{(a)}\oint_I\frac{B}{C}ds+2g_2^{(a)}\oint_{II}\frac{B}{C}ds \\
M_1^{(a)} &= 2g_1^{(a)}A_{eI}+2g_2^{(a)}A_{eII} \\
M_2^{(a)} &= \int_{all}\left(A^{(a)}-\frac{B}{C}C^{(a)}\right)zds \\
&\quad +2g_1^{(a)}\oint_I\frac{B}{C}zds+2g_2^{(a)}\oint_{II}\frac{B}{C}zds \\
M_3^{(a)} &= -\int_{all}\left(A^{(a)}-\frac{B}{C}C^{(a)}\right)yds \\
&\quad -2g_1^{(a)}\oint_I\frac{B}{C}yds-2g_2^{(a)}\oint_{II}\frac{B}{C}yds
\end{aligned}
$$

where the geometric and material terms in these equations can be found in [4].

B Dimensionless terms

The stiffness terms K_{ij} can be non-dimensionalized as:

$$
\begin{aligned}
\Lambda_{11} &= \tfrac{K_{11}}{m\Omega^2L^2} & \Lambda_{12} &= \tfrac{K_{12}}{m\Omega^2L^3} \\
\Lambda_{13} &= \tfrac{K_{13}}{m\Omega^2L^3} & \Lambda_{14} &= \tfrac{K_{14}}{m\Omega^2L^3} \\
\Lambda_{22} &= \tfrac{K_{22}}{m\Omega^2L^4} & \Lambda_{23} &= \tfrac{K_{23}}{m\Omega^2L^4} \\
\Lambda_{24} &= \tfrac{K_{24}}{m\Omega^2L^4} & \Lambda_{33} &= \tfrac{K_{33}}{m\Omega^2L^4} \\
\Lambda_{34} &= \tfrac{K_{34}}{m\Omega^2L^4} & \Lambda_{44} &= \tfrac{K_{44}}{m\Omega^2L^4}
\end{aligned}
$$

Several stiffness terms are grouped together, becoming new constants:

$$
\begin{aligned}
\Gamma_1 &= \left(\Lambda_{33}-\tfrac{\Lambda_{13}^2}{\Lambda_{11}}\right)\sin^2\theta+\left(\Lambda_{34}-\tfrac{\Lambda_{13}\Lambda_{14}}{\Lambda_{11}}\right)\sin 2\theta \\
&\quad +\left(\Lambda_{44}-\tfrac{\Lambda_{14}^2}{\Lambda_{11}}\right)\cos^2\theta \\
\Gamma_2 &= -\left(\Lambda_{33}-\tfrac{\Lambda_{13}^2}{\Lambda_{11}}\right)\cos^2\theta+\left(\Lambda_{34}-\tfrac{\Lambda_{13}\Lambda_{14}}{\Lambda_{11}}\right)\sin 2\theta \\
&\quad -\left(\Lambda_{44}-\tfrac{\Lambda_{14}^2}{\Lambda_{11}}\right)\sin^2\theta \\
\Gamma_3 &= \tfrac{1}{2}\left(\Lambda_{33}-\tfrac{\Lambda_{13}^2}{\Lambda_{11}}\right)\sin 2\theta+\left(\Lambda_{34}-\tfrac{\Lambda_{13}\Lambda_{14}}{\Lambda_{11}}\right)\cos 2\theta \\
&\quad -\tfrac{1}{2}\left(\Lambda_{44}-\tfrac{\Lambda_{14}^2}{\Lambda_{11}}\right)\sin 2\theta \\
\Upsilon_1 &= \left(\Lambda_{23}-\tfrac{\Lambda_{12}\Lambda_{13}}{\Lambda_{11}}\right)\sin\theta+\left(\Lambda_{24}-\tfrac{\Lambda_{12}\Lambda_{14}}{\Lambda_{11}}\right)\cos\theta \\
\Upsilon_2 &= \left(\Lambda_{23}-\tfrac{\Lambda_{12}\Lambda_{13}}{\Lambda_{11}}\right)\cos\theta-\left(\Lambda_{24}-\tfrac{\Lambda_{12}\Lambda_{14}}{\Lambda_{11}}\right)\sin\theta \\
\Pi_1 &= \tfrac{\Lambda_{13}}{\Lambda_{11}}\sin\theta+\tfrac{\Lambda_{14}}{\Lambda_{11}}\cos\theta \\
\Pi_2 &= \tfrac{\Lambda_{13}}{\Lambda_{11}}\cos\theta-\tfrac{\Lambda_{14}}{\Lambda_{11}}\sin\theta
\end{aligned}
$$

The radius of gyrations can be non-dimensionalized as:

$$
\begin{aligned}
\mu &= \tfrac{k_m}{L} \\
\mu_1 &= \tfrac{k_{m_1}}{L} \\
\mu_2 &= \tfrac{k_{m_2}}{L}
\end{aligned}
$$

The non-dimensional aerodynamic constants are given as:

$$
\begin{aligned}
\bar{L_v} &= \tfrac{\gamma}{6}\left\{\bar{v_i}^2-\bar{x}^2\tfrac{C_D}{a}-\bar{x}\bar{v_i}\left(\theta+\bar{\varphi}\right)-\left(2\bar{x}\tfrac{C_D}{a}\right.\right. \\
&\quad \left.\left.+\left(\theta+\bar{\varphi}\right)\bar{v_i}\right)\dot{\bar{v}}+\left(2\bar{v_i}-\bar{x}\left(\theta+\bar{\varphi}\right)\right)\dot{\bar{w}}\right\} \\
\bar{L_w} &= \tfrac{\gamma}{6}\left\{-\bar{x}\bar{v_i}+\bar{x}^2\left(\theta+\bar{\varphi}+\int_0^{\bar{x}}\bar{v}'\bar{w}''d\bar{x}\right)\right. \\
&\quad -\bar{x}\bar{v}\left(\beta_{pc}+\bar{w}'\right)+\tfrac{\bar{x}\bar{c}}{2}\left(\beta_{pc}+\bar{w}'\right) \\
&\quad \left.+\left(2\bar{x}\left(\theta+\bar{\varphi}\right)-\bar{v_i}\right)\dot{\bar{v}}-\bar{x}\dot{\bar{w}}+\tfrac{3}{4}\bar{c}\bar{x}\dot{\bar{\varphi}}-\tfrac{\bar{c}}{4}\ddot{\bar{w}}\right\} \\
\bar{M_\varphi} &= -\tfrac{\gamma}{48}\left(\bar{c}^2\bar{x}\dot{\bar{\varphi}}\right)
\end{aligned}
$$

where γ is the Lock number, given by:

$$\gamma = 3\frac{\rho_{air}a\bar{c}L^2}{m}$$

the dimensionless chord length is:

$$\bar{c} = \frac{c}{L}$$

and the dimensionless inflow velocity is found to be:

$$
\begin{aligned}
\bar{v_i} &= \operatorname{sign}\left[\theta+\varphi_0\left(0.75L\right)\right]\tfrac{\pi\sigma}{8} \\
&\quad \left(\sqrt{1+\tfrac{12}{\pi\sigma}\left|\theta+\varphi_0\left(0.75L\right)\right|}-1\right)
\end{aligned}
$$

C Galerkin variables

$$
\begin{aligned}
A_i &= \int_0^1 \Psi_i d\bar{x} \\
B_i &= \int_0^1 \bar{x}\Psi_i d\bar{x} \\
C_i &= \int_0^1 \bar{x}^2\Psi_i d\bar{x} \\
E_{ij} &= \int_0^1 \bar{x}\Psi_i\Psi_j d\bar{x} \\
G_{ijk} &= \int_0^1 \bar{x}\Psi_i\Psi_j\Theta_k d\bar{x} \\
H_{ijk} &= \int_0^1 \Psi_i\Psi_j\Theta_k d\bar{x} \\
I_{ij} &= \int_0^1 \bar{x}\Psi_i\Theta_j d\bar{x} \\
J_{ij} &= \int_0^1 \bar{x}^2\Psi_i\Theta_j d\bar{x} \\
L_{ijk} &= \int_0^1 \Psi_i\bar{x}\Psi_j\Psi'_k d\bar{x} \\
&\quad -\int_0^1 \Psi_i\bar{x}^2\int_0^{\bar{x}}\Psi'_j\Psi''_k d\bar{x}d\bar{x} \\
M_{ij} &= \int_0^1 \bar{x}\Theta_i\Theta_j d\bar{x} \\
O_{ij} &= \int_0^1 \bar{x}\Psi_i\Psi'_j d\bar{x} \\
P_{ij} &= \int_0^1 \Psi_i\Theta_j d\bar{x} \\
Q_{ij} &= \int_0^1 \bar{x}\left(\Psi_i\Theta_j\right)' d\bar{x} \\
R_{ij} &= \int_0^1 \Psi'''_i\Theta_j d\bar{x}
\end{aligned}
\qquad
\begin{aligned}
S_{ijk} &= -\nu_k^2\int_0^1 \left(\Psi_i\Theta_j\right)'\Theta_k d\bar{x} \\
T_{ij} &= \int_0^1 \Psi_i\Psi'_j d\bar{x} \\
U_i &= \int_0^1 \bar{x}\Theta_i d\bar{x} \\
Y_{ijk} &= \int_0^1 \Psi_i\Psi'_j\Psi_k d\bar{x} \\
Z_i &= \int_0^1 \bar{x}\Psi'_i d\bar{x} \\
\delta_{ij} &= \int_0^1 \Psi_i\Psi_j d\bar{x} \\
&= \int_0^1 \Theta_i\Theta_j d\bar{x} \\
&= \left\{ \begin{array}{ll} 0 & i \neq j \\ 1 & i = j \end{array} \right\} \\
A_{ij}^{(a)} &= \int_0^1 \Psi''_i\mathbf{F}_{1j}^{(a)} d\bar{x} \\
B_{ij}^{(a)} &= \int_0^1 \Psi''_i\mathbf{M}_{3j}^{(a)} d\bar{x} \\
C_{ij}^{(a)} &= \int_0^1 \Psi''_i\mathbf{M}_{2j}^{(a)} d\bar{x} \\
D_{ij}^{(a)} &= \int_0^1 \Theta'_i\mathbf{M}_{1j}^{(a)} d\bar{x} \\
E_{ij}^{(a)} &= \int_0^1 \Theta'_i\mathbf{F}_{1j}^{(a)} d\bar{x}
\end{aligned}
$$

D Steady-state equations

D.1 δV_{0j} equation:

$$
\begin{aligned}
&\sum_{j=0}^{N}\Bigg\{\Gamma_1\beta_j^4\delta_{ij}V_{0j} + \Gamma_3\sum_{k=1}^{N}\left(\beta_j^4H_{ijk} + \beta_i^4H_{ijk}\right)V_{0j}\phi_{0k} - \Gamma_3\beta_j^4\delta_{ij}W_{0j} \\
&+\sum_{k=1}^{N}\left(\Gamma_2\beta_j^4H_{ijk} + \Gamma_1\beta_i^4H_{ijk}\right)W_{0j}\phi_{0k} + \left(O_{ji} + O_{ij} - \delta_{ij}\right)V_{0j} \\
&+\frac{\gamma}{6}\bar{v}_iI_{ij}\phi_{0j} - \Upsilon_1R_{ij}\phi_{0j} - \Upsilon_2\sum_{k=1}^{N}S_{ijk}\phi_{0j}\phi_{0k} + \Pi_2Q_{ij}\phi_{0j} \\
&+\Pi_1E_{e0}A_{ij}^{(a)} - \cos\theta E_{e0}B_{ij}^{(a)} - \sin\theta E_{e0}C_{ij}^{(a)}\Bigg\} \\
&= -\Pi_1Z_i + \frac{\gamma}{6}\left(\bar{v}_i^2A_i - \frac{C_d}{a}C_i - \bar{v}_i\theta B_i\right)
\end{aligned}
$$

D.2 δW_{0j} equation:

$$
\begin{aligned}
&\sum_{j=0}^{N}\Bigg\{-\Gamma_3\beta_j^4\delta_{ij}V_{0j} + \sum_{k=1}^{N}\left(\Gamma_1\beta_j^4H_{ijk} + \Gamma_2\beta_i^4H_{ijk}\right)V_{0j}\phi_{0k} - \Gamma_2\beta_j^4\delta_{ij}W_{0j} \\
&-\Gamma_3\sum_{k=1}^{N}\left(\beta_j^4H_{ijk} + \beta_i^4H_{ijk}\right)W_{0j}\phi_{0k} + \frac{\gamma}{6}\Bigg(\beta_{pc}E_{ij}V_{0j} - \frac{\bar{c}}{2}O_{ij}W_{0j} \\
&-J_{ij}\phi_{0j} + \sum_{k=1}^{N}L_{ijk}V_{0j}W_{0k}\Bigg) + \Upsilon_2R_{ij}\phi_{0j} - \Upsilon_1\sum_{k=1}^{N}S_{ijk}\phi_{0j}\phi_{0k} \\
&+\Pi_1Q_{ij}\phi_{0j} + \left(O_{ij} + O_{ji}\right)W_{0j} - \Pi_2E_{e0}A_{ij}^{(a)} - \sin\theta E_{e0}B_{ij}^{(a)} \\
&-\cos\theta E_{e0}C_{ij}^{(a)}\Bigg\} = -\beta_{pc}B_i + \Pi_2Z_i + \frac{\gamma}{6}\left\{C_i\theta - B_i\bar{v}_i + \frac{\bar{c}}{2}\beta_{pc}B_i\right\}
\end{aligned}
$$

D.3 $\delta\phi_{0j}$ equation:

$$\sum_{j=0}^{N}\left\{\nu_j^2\left(\Lambda_{22}-\frac{\Lambda_{12}^2}{\Lambda_{11}}\right)\delta_{ij}\phi_{0j}+\sum_{k=1}^{N}\beta_k^4\Gamma_3 H_{kji}V_{0j}V_{0k}\right.$$
$$+\Gamma_1\sum_{k=1}^{N}\beta_k^4 H_{kji}W_{0j}V_{0k}-\Gamma_3\sum_{k=1}^{N}\beta_k^4 H_{kji}W_{0j}W_{0k}$$
$$+\Gamma_2\sum_{k=1}^{N}\beta_k^4 H_{kji}V_{0j}W_{0k}+\Pi_2 Q_{ji}V_{0j}+\Pi_1 Q_{ji}W_{0j}$$
$$-\Upsilon_1 R_{ji}V_{0j}-\Upsilon_2\sum_{k=1}^{N}\left(S_{jik}+S_{jki}\right)V_{0j}\phi_{0k}+\Upsilon_2 R_{ji}W_{0j}$$
$$-\Upsilon_1\sum_{k=1}^{N}\left(S_{jik}+S_{jki}\right)W_{0j}\phi_{0k}+\left(\mu_2^2-\mu_1^2\right)\cos(2\theta)\delta_{ij}\phi_{0j}$$
$$\left.-E_{e0}D_{ij}^{(a)}+\frac{\Lambda_{12}}{\Lambda_{11}}E_{e0}E_{ij}^{(a)}\right\}=-\frac{\Lambda_{12}}{\Lambda_{11}}U_i-\frac{1}{\sqrt{2}\nu_i}\left(\mu_2^2-\mu_1^2\right)\sin(2\theta)$$

E Perturbation matrices

$$[M]=\begin{bmatrix}\delta_{ij} & 0 & 0\\ 0 & \delta_{ij}\left(1+\frac{\gamma\bar{c}}{24}\right) & 0\\ 0 & 0 & \mu^2\delta_{ij}\end{bmatrix}$$

$$[C_g]=2\begin{bmatrix}-\Pi_1\left(T_{ij}-T_{ji}\right) & -\beta_{pc}\delta_{ij}+\Pi_2 T_{ij} & -\frac{\Lambda_{12}}{\Lambda_{11}}P_{ij}\\ -\left(Y_{ijk}-Y_{jik}\right)V_{0k} & -\left(Y_{ijk}+Y_{ikj}\right)W_{0k} & \\ \beta_{pc}\delta_{ij}-\Pi_2 T_{ji} & 0 & 0\\ +\left(Y_{jik}+Y_{ikj}\right)W_{0k} & & \\ \frac{\Lambda_{12}}{\Lambda_{11}}P_{ji} & 0 & 0\end{bmatrix}$$

$$[C_a]=\frac{\gamma}{6}\begin{bmatrix}2\frac{C_D}{a}E_{ij}+\theta\bar{v}_i\delta_{ij} & 2\bar{v}_i\delta_{ij}-\theta E_{ij} & 0\\ +\bar{v}_i\sum_{k=1}^{N}H_{ijk}\phi_{0k} & -\sum_{k=1}^{N}G_{ijk}\phi_{0k} & \\ \bar{v}_i\delta_{ij}-2\theta E_{ij} & E_{ij} & -\frac{3\bar{c}}{4}I_{ij}\\ -2\sum_{k=1}^{N}G_{ijk}\phi_{0k} & & \\ 0 & 0 & \frac{\bar{c}^2}{8}M_{ij}\end{bmatrix}$$

$$[K_a]=\frac{\gamma}{6}\begin{bmatrix}0 & 0 & \bar{v}_i I_{ij}\\ \beta_{pc}E_{ij}+\sum_{k=1}^{N}L_{ijk}W_{0k} & -\frac{\bar{c}}{2}O_{ij}+\sum_{k=1}^{N}L_{ikj}V_{0k} & -J_{ij}\\ 0 & 0 & 0\end{bmatrix}$$

$$\{F\}=\sum_{j=1}^{N}\begin{Bmatrix}\Pi_1 A_{ij}^{(a)}-\cos\theta B_{ij}^{(a)}-\sin\theta C_{ij}^{(a)}\\ -\Pi_2 A_{ij}^{(a)}-\sin\theta B_{ij}^{(a)}-\cos\theta C_{ij}^{(a)}\\ -D_{ij}^{(a)}+\frac{\Lambda_{12}}{\Lambda_{11}}E_{ij}^{(a)}\end{Bmatrix}$$

$$
[K_s] \quad = \quad \left[\begin{array}{ccc}
\begin{array}{c} \beta_j^4 \Gamma_1 \delta_{ij} + O_{ij} + O_{ji} - \delta_{ij} \\ + \Gamma_3 \left(\beta_j^4 + \beta_i^4 \right) \sum_{k=1}^{N} H_{ijk} \phi_{0k} \end{array} & \begin{array}{c} \left(\beta_i^4 \Gamma_1 + \beta_j^4 \Gamma_2 \right) \sum_{k=1}^{N} H_{ijk} \phi_{0k} \\ - \beta_j^4 \Gamma_3 \delta_{ij} \end{array} & \begin{array}{c} \Gamma_3 \sum_{k=1}^{N} \left(\beta_k^4 + \beta_i^4 \right) H_{ikj} V_{0k} \\ + \sum_{k=1}^{N} \left(\beta_k^4 \Gamma_2 + \beta_i^4 \Gamma_1 \right) H_{ikj} W_{0k} \\ - \Upsilon_1 R_{ij} + \Pi_2 Q_{ij} \\ - \Upsilon_2 \sum_{k=1}^{N} \left(S_{ijk} + S_{ikj} \right) \phi_{0k} \end{array} \\
\begin{array}{c} \left(\Gamma_1 \beta_j^4 + \Gamma_2 \beta_i^4 \right) \sum_{k=1}^{N} H_{ijk} \phi_{0k} \\ - \beta_j^4 \Gamma_3 \delta_{ij} \end{array} & \begin{array}{c} - \Gamma_3 \sum_{k=1}^{N} \left(\beta_j^4 + \beta_i^4 \right) H_{ijk} \phi_{0k} \\ + O_{ij} + O_{ji} - \beta_j^4 \Gamma_2 \delta_{ij} \end{array} & \begin{array}{c} \sum_{k=1}^{N} \left(\beta_k^4 \Gamma_1 + \beta_i^4 \Gamma_2 \right) H_{ikj} V_{0k} \\ - \Gamma_3 \sum_{k=1}^{N} \left(\beta_k^4 + \beta_i^4 \right) H_{ikj} W_{0k} \\ + \Upsilon_2 R_{ij} + \Pi_1 Q_{ij} \\ - \Upsilon_1 \sum_{k=1}^{N} \left(S_{ijk} + S_{ikj} \right) \phi_{0k} \end{array} \\
\begin{array}{c} \Gamma_3 \sum_{k=1}^{N} \left(\beta_k^4 H_{kji} + \beta_j^4 H_{jki} \right) V_{0k} \\ + \sum_{k=1}^{N} \left(\Gamma_1 \beta_j^4 H_{jki} + \Gamma_2 \beta_k^4 H_{kji} \right) W_{0k} \\ - \Upsilon_1 R_{ji} + \Pi_2 Q_{ji} \\ - \Upsilon_2 \sum_{k=1}^{N} \left(S_{jik} + S_{jki} \right) \phi_{0k} \end{array} & \begin{array}{c} \sum_{k=1}^{N} \left(\Gamma_1 \beta_k^4 H_{kji} + \Gamma_2 \beta_j^4 H_{jki} \right) V_{0k} \\ - \Gamma_3 \sum_{k=1}^{N} \left(\beta_k^4 H_{kji} + \beta_j^4 H_{jki} \right) W_{0k} \\ + \Upsilon_2 R_{ji} + \Pi_1 Q_{ji} \\ - \Upsilon_1 \sum_{k=1}^{N} \left(S_{jik} + S_{jki} \right) \phi_{0k} \end{array} & \begin{array}{c} \nu_j^2 \left(\Lambda_{22} - \frac{\Lambda_{12}^2}{\Lambda_{11}} \right) \delta_{ij} \\ + \left(\mu_2^2 - \mu_1^2 \right) \cos\left(2\theta \right) \delta_{ij} \\ - \Upsilon_2 \sum_{k=1}^{N} \left(S_{kji} + S_{kij} \right) V_{0k} \\ - \Upsilon_1 \sum_{k=1}^{N} \left(S_{kji} + S_{kij} \right) W_{0k} \end{array}
\end{array} \right]
$$